

# Future Improvement to Search for Muon to Positron Conversion in a Muonic Atom

Beomki Yeo<sup>a,\*</sup>, Yoshitaka Kuno<sup>b</sup>, MyeongJae Lee<sup>c</sup>, Kai Zuber<sup>d</sup>

<sup>a</sup>*Department of Physics, Korea Advanced Institute of Science and Technology (KAIST),  
Daejeon 34141, Republic of Korea*

<sup>b</sup>*Department of Physics, Graduate School of Science, Osaka University,  
Toyonaka, Osaka 560-0043, Japan*

<sup>c</sup>*Center for Axion and Precision Physics Research, Institute for Basic Science (IBS),  
Daejeon 34051, Republic of Korea*

<sup>d</sup>*Institute for Nuclear and Particle Physics, Technische Universität Dresden, Germany*

---

## Abstract

This paper discusses how to improve the experimental sensitivity of the  $\mu^- + N(A, Z) \rightarrow e^+ + N(A, Z - 2)$  conversion in a muonic atom, which is a charged lepton number and lepton flavor violating (CLNLFV) process. Currently, the measurement of this process is planned with future experiments to search for the  $\mu^- - e^-$  conversion with an aluminum target. We demonstrate that a search for  $\mu^- - e^+$  would be limited to a sensitivity improvement less than a factor of ten due to backgrounds from radiative muon capture, whereas the  $\mu^- - e^-$  conversion is anticipated to have four orders of magnitude of improvement in its experimental sensitivity. We propose new measurements to achieve the improvement of four orders of magnitude also for the  $\mu^- - e^+$  conversion by using new target materials, which should meet the requirement of  $M(A, Z - 2) < M(A, Z - 1)$  for the mass of the target nucleus of  $M(A, Z)$ .

**Keywords:** charged lepton flavor violation, lepton number violation, muon to positron conversion

**PACS:** 13.35.Bv, 14.60.Ef, 36.10.Ee

---

## 1. Introduction

Neutrino masses and mixing are among the most important issues in particle physics. New particles and interactions beyond the Standard Model (SM) are required to explain these issues. As the mixing of neutrinos was confirmed by the discovery of neutrino oscillation, much interest has moved to charged leptons in terms of the search for new physics beyond the SM. Although the processes of charged lepton flavor violation (CLFV) can occur by neutrino mixing in the SM, the rates of the SM contributions are found to be extremely small, in the order of  $\mathcal{O}(10^{-54})$  due to small neutrino masses. On the other hand, most extensions of the SM, such as supersymmetric (SUSY) models, can predict sizable rates of the CLFV processes [1]. They have been investigated through the various muon decay channels:  $\mu^- \rightarrow e^-$  conversion,  $\mu^- \rightarrow e^- + \gamma$  decay and  $\mu^- \rightarrow e^- + e^- + e^+$  decay [1] in the expectation of the discovery of New Physics. Another process is lepton number violation (LNV), which has been mostly examined by neutrinoless double beta decays ( $0\nu\beta\beta$ ). The LNV processes, with the change of lepton number by two units, can be mediated by Majorana neutrinos or new particles appearing at a high energy scale. They are also direct channels in the search for the effective Majorana masses ( $\langle m_{\alpha\beta} \rangle$ ), which are defined by  $\langle m_{\alpha\beta} \rangle = \left| \sum_{k=1}^3 U_{\alpha k} U_{\beta k} m_k \right|$  with  $\alpha, \beta = e, \mu, \tau$ , where  $U_{ij}$  are the neutrino mixing matrix elements, and  $m_k$  are the neutrino mass eigenvalues. The Majorana nature of neutrino masses, in particular  $\langle m_{ee} \rangle$ , can be proved by the  $0\nu\beta\beta$  processes regardless of the type of mediating particles according to the Schechter-Valle theorem [2]. It is a remarkable aspect because the existence of Majorana neutrinos could resolve the origin of the small neutrino mass problem through the seesaw mechanism. However, there is a limitation

---

\*Corresponding author

Email addresses: byeo@kaist.ac.kr (Beomki Yeo), kuno@phys.sci.osaka-u.ac.jp (Yoshitaka Kuno), myeongjaelee@ibs.re.kr (MyeongJae Lee), zuber@physik.tu-dresden.de (Kai Zuber)

Table 1: The upper limits (as 90% C.L.) on the  $\mu^- - e^+$  conversion of the past experiments. The experiments with the best upper limit on each target are listed. (\*) denotes the excited nucleus after the conversion.

Year	Process	Upper limit	Ref
1972	$\mu^- + \text{Cu} \rightarrow e^+ + \text{Co}$	$2.6 \times 10^{-8}$	[7]
1980	$\mu^- + \text{I} \rightarrow e^+ + \text{Sb}^*$	$3.0 \times 10^{-10}$	[9]
1982	$\mu^- + \text{S} \rightarrow e^+ + \text{Si}^*$	$9.0 \times 10^{-10}$	[10]
1998	$\mu^- + \text{Ti} \rightarrow e^+ + \text{Ca}$	$1.7 \times 10^{-12}$	[13]
	$\mu^- + \text{Ti} \rightarrow e^+ + \text{Ca}^*$	$3.6 \times 10^{-11}$	

that  $0\nu\beta\beta$  decay experiments are not sensitive to identifying the exact mechanism of the neutrino mass generation.

The observation of the  $\mu^- + N(A, Z) \rightarrow e^+ + N(A, Z - 2)$  conversion can shed light on both kinds of physics at the same time because this conversion requires the charged lepton number and flavor violation (CLNFV). Some theories beyond the SM of particle physics, such as the Majorana neutrino, the doubly charged singlet scalar model, and the left-right symmetric model, have been suggested as feasible theories for the  $\mu^- - e^+$  conversion [3] while the Majorana neutrino exchange model through the type-1 seesaw mechanism is hardly observable with bounds from the neutrino masses and the mixing angles known so far [4]. Thus, if the  $\mu^- - e^+$  conversion is observed with the achievable sensitivity of coming experiments, the neutrino masses might originate from other mechanisms dominantly rather than the Majorana neutrino exchange, especially for the doubly charged singlet scalar model [5, 6]. This means that the physical scope of the  $\mu^- - e^+$  conversion experiment on the neutrino mass generation mechanism is more specified than the  $0\nu\beta\beta$  decay experiment is. However, it should be noted that the observation of the  $\mu^- - e^+$  conversion, analogous to the  $0\nu\beta\beta$  process, will eventually imply the nonzero  $\langle m_{e\mu} \rangle$  irrespective of the physics behind, which evidently reveals the Majorana nature of neutrino masses.

Nuclear physics as well as particle physics models comes into play since the  $\mu^- - e^+$  conversion changes an atomic number of the nucleus by two units. In other words, the  $\mu^- - e^+$  conversion is associated with nuclear interaction, which is represented as the nuclear matrix element in the calculation of the decay rate. Another aspect of nuclear interaction is that the nucleus in the final state after the  $\mu^- - e^+$  conversion is divided into two cases in which a daughter nucleus stays in the ground state or enters excited states. In this work, we focus on the case of the ground state since excited states suffer more from background influence, and the energy distribution of the signals for excited states is not known well due to the uncertainty of nuclear physics.

The current limits on the  $\mu^- - e^+$  conversion based on past experiments are summarized in Table 1 [7–13]. Currently, there are two planned experiments where the measurements of the  $\mu^- - e^+$  conversion can be possibly made: COMET and Mu2e<sup>1</sup>, which were originally designed to search for the  $\mu^- - e^-$  conversion with four orders of magnitude of improvement over the current limit, namely  $\sim O(10^{-16})$  with an aluminum muon-stopping target [14–16]. However, as we will see later, the improvement of  $\mu^- - e^+$  conversion sensitivity may be considerably limited by the background from radiative muon capture (RMC). In this study, this kind of limitation was overcome by selecting the proper muon-stopping target material, other than aluminum, which suppresses the RMC background.

The remainder of this letter is organized as following: In Sec. 2, we describe a generic  $\mu^- - e^+$  conversion experiment. In Sec. 3, we estimate the background, and claim that RMC is the dominating background for an aluminum muon-stopping target. In Sec. 4, we introduce candidate stopping target materials which improve the sensitivity by four orders of magnitude. The summary follows in Sec. 5.

## 2. Experimental aspects of $\mu^- - e^+$ signal detection

The experimental method of  $\mu^- - e^+$  conversion is summarized as follows. A pulsed proton beam hits a pion production target to generate a bunch of pions. The negative pions are captured by a solenoidal magnetic field and sent to a muon-stopping target, while most of the pions decay into muons during transport. These muons are stopped

<sup>1</sup>Both of the COMET Phase-1 and the Mu2e experiments can measure the  $\mu^- - e^+$  and  $\mu^- - e^-$  conversion simultaneously while the COMET Phase-2 experiment may need to change the polarity of the dipole magnetic field in the detector solenoid.

at the muon-stopping target forming a muonic atom, and subsequently cascade down to 1s ground state, followed by muon decays in the 1s orbit of a muonic atom (decay-in-orbit=DIO) and muon capture by a nucleus. If the  $\mu^- - e^+$  conversion occurs, a single positron is emitted, and the measurement of the single positron is the signature of the process. For the transition to the ground state of the daughter nucleus, the signal positron is mono-energetic. Its energy is given by

$$E_{\mu^-e^+} = m_\mu + M(A, Z) - M(A, Z - 2) - B_\mu - E_{recoil}, \quad (1)$$

where  $m_\mu$ ,  $B_\mu$ , and  $E_{recoil}$  are the muon mass, the 1s binding energy of the muonic atom, and the recoil energy of the nucleus, respectively. Here,  $M(A, Z)$  is the mass of the target nucleus, and  $M(A, Z - 2)$  is the mass of the daughter nucleus. The momenta of the signal positrons are measured at the detector for their identification.

The single event sensitivity (SES) of the  $\mu^- - e^+$  conversion, which corresponds to the sensitivity of the experiment in a background-free case, is given by

$$SES = \frac{1}{N_p \times R_{\text{stopped } \mu^-/p} \times f_{cap} \times \mathcal{E}}, \quad (2)$$

where  $N_p$  is the total number of protons,  $R_{\text{stopped } \mu^-/p}$  is the number of stopped muons per proton,  $f_{cap}$  is the nuclear muon capture rate (for example, 0.61 for aluminum), and  $\mathcal{E}$  is the positron acceptance rate. The sensitivity of the  $\mu^- - e^+$  conversion is usually lower than that of the  $\mu^- - e^-$  conversion for several reasons. First of all, in the  $\mu^- - e^+$  conversion, the initial-state nucleus and the final-state nucleus are different; therefore, no enhancement due to coherence exists, whereas in the  $\mu^- - e^-$  conversion, there exists coherent enhancement for the transition to the ground state. This enhancement is in the order of the number of nucleons ( $A$ ). Secondly, as a byproduct search, the detector is optimized to the detection of electrons, not positrons. This results in smaller detector acceptance, although it can be overcome by a dedicated experimental setup.

### 3. Background estimation

Processes other than the  $\mu^- - e^\pm$  conversion are background sources. The first background source is the charge misidentification of DIO electrons. Considering that the momentum resolution  $\Delta p/p$  of the current experiments (COMET and Mu2e) is less than 0.1%, the geometrical helicity of the charged particle is hardly misidentified. However, the actual charge misidentification rate of each experiment should be carefully understood because the DIO energy spectrum rapidly increases at lower energy. The second background comes from the RMC which emits a high energy photon. When this is followed by an asymmetric pair production ( $\gamma \rightarrow e^- + e^+$ ), the emitted positron can fake the  $\mu^- - e^+$  signal if the endpoint energy of a positron from RMC ( $E_{RMC}^{end}$ ) is higher than  $E_{\mu^-e^+}$ . The pions contaminating the muon beam are another background source. Such pions are captured by the muon-stopping target followed by photon emission, called radiative pion capture (RPC), with 1–2 % probability for atoms ( $^{12}\text{C}$ ,  $^{16}\text{O}$  and  $^{40}\text{Ca}$ ) investigated in Ref. [17]. Since the pion mass (139.57 MeV) is higher than the muon mass (105.66 MeV), RPC is capable of generating fake positron signals. In the following subsections, we estimate each background with a muon-stopping target made of aluminum for a detector, which is similar to the baseline design of the COMET and Mu2e experiments.

#### 3.1. DIO background

Let us consider first the background from the charge misidentification of DIO electrons. The endpoint energy of DIO is given by

$$E_{DIO}^{end} = m_\mu - B_\mu - E_{recoil}. \quad (3)$$

The number of accepted DIO electrons ( $N_{DIO}$ ) whose energy is higher than a lower bound ( $E_{min}$ ) is given by

$$N_{DIO} \sim N_p \times R_{\text{stopped } \mu^-/p} \times Br(\text{DIO}) \times \mathcal{E} \times P_{e^- \rightarrow e^+}, \quad (4)$$

where  $Br(\text{DIO})$  is the branching ratio of DIO from  $E_{min}$  to  $E_{DIO}^{end}$  (104.97 MeV for aluminum),  $\mathcal{E}$  is the electron acceptance rate assumed to be a constant for a given energy range, and  $P_{e^- \rightarrow e^+}$  is the charge misidentification rate. Here,  $Br(\text{DIO})$  can be obtained numerically from the spectrum of DIO for aluminum [18] near the endpoint energy,

and is found to be  $6.77 \times 10^{-10}$  in an energy range from 90.30 MeV to 104.97 MeV.

As a next step,  $10^8$  DIO electrons with this energy range are generated to estimate the charge misidentification rate. The lower bound (90.30 MeV) is determined conservatively by subtracting 2 MeV from the  $\mu^- - e^+$  signal energy (92.30 MeV) in aluminum. The trajectory of each particle follows a simple helix in a 1 T magnetic field composed of 20 spatial points with 16 mm intervals. All spatial points of the hits ( $x, y, z$ ) are smeared with a finite resolution (200  $\mu\text{m}$ , 200  $\mu\text{m}$ , 3 mm, respectively) because the detection in the longitudinal direction of particle motion ( $z$ ) is usually low. The smeared hits are fitted into the helical trajectory by using GENFIT [19], and the charges of the generated particles are identified from the geometrical helicity of the fitted trajectory. More than 99.99% of the DIO electrons have a fitted momentum between 80 MeV and 105 MeV, and no charge misidentification is found in that momentum range. Hence, the charge misidentification rate ( $P_{e^- \rightarrow e^+}$ ) is lower than  $1.0 \times 10^{-8}$ , which is enough to make the DIO background negligible in the  $\mu^- - e^+$  detection. The scale of  $N_{DIO}$  can be estimated by putting appropriate values into Eq. (4):  $N_p$ ,  $R_{\text{stopped } \mu^-/p}$ , and  $\mathcal{E}$  are set to  $10^{21}$ ,  $10^{-3}$ , and  $10^{-2}$ , respectively, to achieve SES of  $\mathcal{O}(10^{-16})$  for the  $\mu^- - e^+$  conversion from Eq. (2). With these values,  $N_{DIO}$  is less than  $6.77 \times 10^{-2}$ .

### 3.2. RMC background

The background from RMC is more intrinsic, so it is difficult to get rid of it in a technical way. The endpoint energy of RMC is given by

$$E_{RMC}^{end} = m_\mu + M(A, Z) - M(A, Z - 1) - B_\mu - E_{recoil}, \quad (5)$$

where  $M(A, Z - 1)$  is the mass of the daughter nucleus after RMC. The energy spectrum of an RMC photon can be approximated as [20]

$$P(x) \simeq C(1 - 2x + 2x^2)x(1 - x)^2, \quad x = \frac{E_\gamma}{E_\gamma^{end}}, \quad (6)$$

where the normalization constant  $C$  can be determined based on previous experiments [21–23], and  $E_\gamma^{end}$  is the endpoint energy of RMC photons. In each experiment, the experimental value of  $E_\gamma^{end}$  was obtained by fitting the photon energy distribution in the shape of Eq. (6). Those fitted spectra used to have the experimental value of  $E_\gamma^{end}$  around 10 MeV smaller than the theoretical endpoint energy, which is calculated based on kinematics. Regarding this discrepancy, Eq. (6) was actually developed from the closure approximation in which the excitation energy of a nucleus is averaged into a single energy. There have been theoretical attempts to make a correction to this spectrum assuming that the final nuclei are excited with dipole resonance or higher resonance modes within the nuclear collective model [24, 25]. However, because there still remains an uncertainty in the nuclear excitation model, we utilize Eq. (6) with the kinematical endpoint energy (101.85 MeV for aluminum) for conservative estimation. The number of accepted positrons from RMC ( $N_{RMC}$ ) above  $E_{min}$  is summarized by

$$N_{RMC} \sim N_p \times R_{\text{stopped } \mu^-/p} \times Br(RMC) \times P_{\gamma \rightarrow e^- + e^+} \times P_{V \subset T} \times P_{E_{e^+} > E_{min}} \times \mathcal{E}, \quad (7)$$

where  $Br(RMC)$  is the branching ratio of RMC whose photon energy is higher than  $E_{min}$ ,  $P_{\gamma \rightarrow e^- + e^+}$  is the probability of a pair production,  $P_{E_{e^+} > E_{min}}$  is the probability that a positron from the pair production has energy higher than  $E_{min}$ , and  $P_{V \subset T}$  is the probability that a pair production vertex is located inside the stopping target. Here,  $P_{V \subset T}$  is supposed to be considered because the events that the pair production vertex is located outside the stopping target can be avoided by using the extrapolation of the trajectory of the daughter particles. Here,  $Br(RMC)$  has the value of  $6.82 \times 10^{-7}$  assuming an energy range from 90.30 MeV to 101.85 MeV based on the result of Ref. [21].

Simulation studies [26] are carried out to get the values of other parameters. First,  $10^7$  photons with the RMC spectrum are generated above 90.30 MeV ( $E_{min}$ ) inside aluminum stopping targets. The stopping targets are composed of 17 flat disks whose radius is 100 mm, thickness is 200  $\mu\text{m}$ , and the spacing between disks is 50 mm, which benchmarks the design of COMET target [15]. It is the general standard because the Mu2e target also has the same specifications except that the radius of the disks gets smaller uniformly from 83 mm to 65 mm [16]. Simulation result shows that  $P_{\gamma \rightarrow e^- + e^+}$  is 0.96,  $P_{V \subset T}$  is 0.0058, and  $P_{E_{e^+} > E_{min}}$  is 0.016. With the given values,  $N_{RMC}$  is expected to be  $5.54 \times 10^5$ , which is seven orders of magnitude higher than  $N_{DIO}$ .

For an illustrative purpose, Fig. 1 shows the estimation of the energy spectrum of the RMC background and the  $\mu^- - e^+$  signal positron with a  $1.7 \times 10^{-12}$  signal branching ratio, which is the current limit. To estimate how much

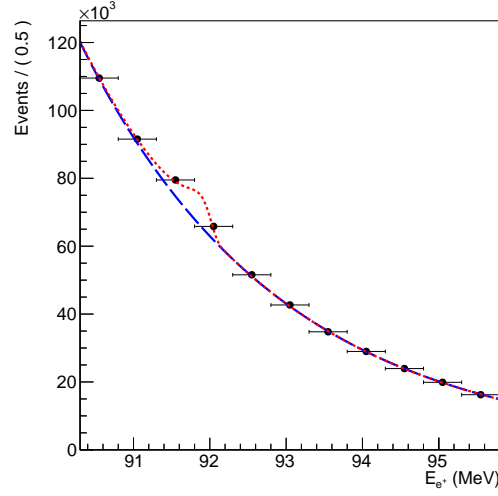


Figure 1: Expected energy histogram of the  $\mu^- - e^+$  signal (red and short dashed line) stacked on the on-shell RMC photon background (blue and long dashed line). The  $\mu^- - e^+$  conversion branching ratio is set to  $1.7 \times 10^{-12}$ . Black dots represent the randomly generated positrons from the background and signal model. Signal spectrum is shifted to the lower energy side because of the energy loss in the stopping targets.

the sensitivity would be improved over the current limit, the statistical significance of the signal with a given signal branching ratio is examined using a maximum likelihood method. The other background factors and systematical uncertainties are assumed to be negligible, and the energy range from 90.30 MeV to 95.8 MeV is considered to reduce the uncertainty at the high energy side. With this assumption, the signal branching ratio that has  $3\sigma$  significance under the null hypothesis is found to be  $2.8 \times 10^{-13}$ .

We estimated the background of an on-shell photon from RMC, but there is the probability that internal conversion could occur with an off-shell photon. Since there has been no study on the energy spectrum of positrons emitted by the internal conversion, the amount of background is conservatively assumed to be the same as the on-shell RMC background. In that case, the signal branching ratio of  $4.0 \times 10^{-13}$  is found to have  $3\sigma$  significance. These results imply that sensitivity improvement of more than a factor of ten may not be achieved, which requires at least  $1.7 \times 10^{-13}$  signal branching ratio.

### 3.3. RPC background

RPC is the beam-related background where (1) the pions decay from the protons out of the main beam bunches, or (2) the pions slowly come from the main beam bunches. The latter case can be suppressed by delaying the detection time window benefiting from the short lifetime of pions (26 ns). In the former case,  $N_{RPC}$  above  $E_{min}$  is estimated using the similar method as for the RMC background:

$$N_{RPC} \sim N_p \times R_{ext} \times R_{\text{stopped } \pi^-/p} \times Br(RPC) \times P_{\gamma \rightarrow e^- + e^+} \times P_{VCT} \times P_{E_{e^+} > E_{min}} \times \mathcal{E}, \quad (8)$$

where  $R_{ext}$  is the extinction factor, which is the ratio of the number of protons out of the beam bunch to the total number of protons, and  $R_{\text{stopped } \pi^-/p}$  is the number of stopped pions per proton.  $P_{\gamma \rightarrow e^- + e^+}$ ,  $P_{VCT}$  and  $P_{E_{e^+} > E_{min}}$  are 0.97, 0.0057, and 0.14, respectively when they are estimated by the generation of  $10^5$  photons at the stopping targets.<sup>2</sup> Assuming  $R_{ext}$  of  $10^{-10}$  and  $R_{\text{stopped } \pi^-/p}$  of  $10^{-7}$  based on the specification of the current experiments,  $N_{RPC}$  is expected to be  $1.55 \times 10^{-3}$ . The contribution of the RPC background is extremely small compared to the RMC background. Internal conversion occurs for RPC as well, but we assume that its contribution is approximately the same as that of the on-shell photon background from RPC.

<sup>2</sup>The RPC spectrum of  $^{40}\text{Ca}$  [17] is used because there is no experimental data for aluminum.

Table 2: Stopping-target material candidates whose  $E_{\mu^-e^+}$  values are higher than, or comparable to,  $E_{RMC}^{end}$ , or equivalently  $M(A, Z-2) < M(A, Z-1)$ . If more than two isotopes satisfy the criteria, only one isotope with the highest natural abundance (N.A.) is listed. Here,  $E_{RMC,n}^{end}$  is the kinematical endpoint energy of the positron from the RMC with  $n$  multiplicity. Nuclear masses required for calculation are referred from AME 2012 data [27]. Here, ( $\dagger$ ) means that the nucleus was already used for previous  $\mu^- - e^+$  conversion experiments. Aluminum does not meet the criteria, but it is stated for comparison.

Atom	$E_{\mu^-e^+}$ (MeV)	$E_{DIO}^{end}$ (MeV)	$E_{RMC,0}^{end}$ (MeV)	$E_{RMC,1}^{end}$ (MeV)	$E_{RMC,2}^{end}$ (MeV)	$E_{RMC,3}^{end}$ (MeV)	N.A. (%)	$f_{cap}$ (%)	$\tau_{\mu^-}$ (ns)
$^{27}\text{Al}$	92.30	104.97	101.34	94.92	83.86	76.55	100	60.95	864.0
$^{32}\text{S}^\dagger$	101.80	104.76	102.03	94.11	81.83	70.54	94.99	75.00	554.7
$^{40}\text{Ca}$	103.55	104.39	102.06	94.27	81.23	69.18	96.94	85.07	332.7
$^{48}\text{Ti}^\dagger$	98.89	104.18	99.17	90.95	80.32	71.58	73.72	85.29	329.3
$^{50}\text{Cr}$	104.06	103.92	101.86	92.55	81.01	70.49	4.35	89.39	233.7
$^{54}\text{Fe}$	103.30	103.65	101.93	93.01	80.97	70.45	5.85	90.85	206
$^{58}\text{Ni}$	104.25	103.36	101.95	93.39	82.03	71.96	68.08	93.06	152.3
$^{64}\text{Zn}$	103.10	103.04	101.43	93.53	82.68	73.82	48.27	92.99	159.4
$^{70}\text{Ge}$	100.67	102.70	100.02	92.38	82.08	73.81	20.84	92.72	166.5

#### 4. Search for the optimal target material

As shown in the previous sections, an aluminum target may suffer from the RMC background severely, and the improvement of sensitivity is limited by a factor less than ten. As a matter of fact, aluminum is one of the worst target materials for the measurement of the  $\mu^- - e^+$  conversion. However, if an appropriate target is selected so that the endpoint energy of the RMC background ( $E_{RMC}^{end}$ ) is lower than the signal energy of the  $\mu^- - e^+$  conversion ( $E_{\mu^-e^+}$ ), the RMC background would not be problem, that is,  $E_{RMC}^{end} < E_{\mu^-e^+}$ . From Eqs. (1) and (5), the criteria for the selection of a new target material of  $M(A, Z)$  is that  $M(A, Z-2) < M(A, Z-1)$  in the case without any nucleon emission in the final state. In the case of RMC with nucleon emission, the additional emitted particles can be neutrons or charged particles, such as protons, alpha particles, and deuterons. RMC with nucleon emission also can generate background positrons if its endpoint energy is higher than  $E_{\mu^-e^+}$ .

Neutron emission is one of the most common processes in muon capture physics. Its probability is higher than 60% for atoms investigated in Ref. [28], so the endpoint energy of this process should be checked with neutron multiplicity. Since the probability of neutron emission with its multiplicity more than four is usually lower than 10% [28], it is sufficient to take into account multiplicity up to three. In contrast, the background from charged particle emission can be excluded because the probability of this process is less than 20% according to the results of Ref. [29, 30]. Besides, most events are accompanied by neutron emission. Table 2 shows a list of candidate target materials with atomic mass  $\leq 70$ , which satisfy the requirements. In Table 2, it is seen that the RMC endpoint energies with neutron emission are lower than that with no emission, and also they decrease further as the neutron multiplicity increases. This tendency can be explained by the binding energy per nucleon of usually 7–9 MeV.

There are other requirements from an experimental points of view. For instance, the muon capture rate ( $f_{cap}$ ) and the muon lifetime ( $\tau_{\mu^-}$ ) of each nucleus are listed [31, 32] because they are important in determining the timing window of signal positron measurement in the pulsed muon beam experiment. Natural abundance is another important characteristic in target selection. If a muon-stopping target is fabricated with a material existing in nature, the background from other isotopes can perturb the signal. For example, titanium in nature is composed of five isotopes ( $A=46, 47, 48, 49, 50$ ). The RMC endpoint energy of  $^{46}\text{Ti}$ , whose natural abundance is 8.25%, is 100.79 MeV, which is higher than the  $\mu^- - e^+$  signal energy of  $^{48}\text{Ti}$ , so it is possible that the signal is blurred by the RMC background. It is also evident that the signal itself is dispersed into a broader spectrum as long as the natural abundance of the candidate isotope is not high enough. In order to avoid this problem, a specific isotope should be enriched. Chemical properties also should be considered because, if a material is reactive, it is hard to prevent the target being contaminated by impurities. As an example, alkali and alkaline earth metals, such as calcium, need caution in fabrication and storage. Considering those features,  $^{32}\text{S}$  can stand as one of the potential candidates because of its relatively high natural abundance and sustainability as a pure target. For these suitable target materials, we could go down to  $O(10^{-16})$  in the

experimental sensitivity of the  $\mu^- - e^+$  conversion, which would be four orders of magnitude of improvement over the current limit.

## 5. Summary

We discussed how we could improve the experimental sensitivity of the  $\mu^- - e^+$  conversion against its background events in the upcoming CLFV experiments with the selection of a dedicated target material. It should be noted that this study focused on the case of transition to the ground state after the  $\mu^- - e^+$  conversion since it could be background-free where transitions to excited states suffer from background influences. We proposed new measurements to achieve improvement of four orders of magnitude for the  $\mu^- - e^+$  conversion by using new target materials, which should meet the requirement of  $M(A, Z - 2) < M(A, Z - 1)$  with the mass of the target nucleus of  $M(A, Z)$ . A tentative appropriate target material could be sulfur among the other candidates available.

## Acknowledgements

This work of B.Y. and M.L. was supported by the Institute for Basic Science of Republic of Korea (project number: IBS-R017-D1). This work of Y.K. was supported in part by the Japan Society of the Promotion of Science (JSPS) KAKENHI Grant No. 25000004. We would like to thank the National Institute of Nuclear and Particle Physics (IN2P3) for providing the computing resources.

## References

- [1] Y. Kuno, Y. Okada, Muon decay and physics beyond the standard model, *Rev. Mod. Phys.* 73 (2001) 151–202.
- [2] J. Schechter, J. W. F. Valle, Neutrinoless double- $\beta$  decay in  $SU(2) \times U(1)$  theories, *Phys. Rev. D* 25 (1982) 2951–2954.
- [3] T. Geib, A. Merle, K. Zuber,  $\mu^- - e^+$  conversion in upcoming LFV experiments, *Phys. Lett. B* 764 (2017) 157 – 162.
- [4] P. Domin, et al., Nuclear ( $\mu^-$ ,  $e^+$ ) conversion mediated by Majorana neutrinos, *Phys. Rev. C* 70 (2004) 065501.
- [5] C. S. Chen, C. Q. Geng, J. N. Ng, Unconventional neutrino mass generation, neutrinoless double beta decays, and collider phenomenology, *Phys. Rev. D* 75 (2007) 053004.
- [6] S. F. King, A. Merle, L. Panizzi, Effective theory of a doubly charged singlet scalar: complementarity of neutrino physics and the LHC, *J. High Energy Phys.* 2014 (11) (2014) 124.
- [7] D. A. Bryman, et al., Search for the Reaction  $\mu^- + \text{Cu} \rightarrow e^+ + \text{Co}$ , *Phys. Rev. Lett.* 28 (1972) 1469 – 1471.
- [8] A. Badertscher, et al., Search for  $\mu^- \rightarrow e^+$  conversion on sulfur, *Phys. Lett. B* 79 (4) (1978) 371 – 375.
- [9] R. Abela, et al., New upper limit for  $\mu^- \rightarrow e^+$  conversion, *Phys. Lett. B* 95 (2) (1980) 318 – 322.
- [10] A. Badertscher, et al., A search for muon-electron and muon-positron conversion in sulfur, *Nucl. Phys. A* 377 (2) (1982) 406 – 440.
- [11] S. Ahmad, et al., Search for muon-electron and muon-positron conversion, *Phys. Rev. D* 38 (1988) 2102 – 2120.
- [12] C. Dohmen, et al., Test of lepton-flavour conservation in  $\mu \rightarrow e$  conversion on titanium, *Phys. Lett. B* 317 (4) (1993) 631 – 636.
- [13] J. Kaulard, et al., Improved limit on the branching ratio of  $\mu^- \rightarrow e^+$  conversion on titanium, *Phys. Lett. B* 422 (14) (1998) 334 – 338.
- [14] R. Abramishvili, et al., COMET Phase 1 Technical Design Report, KEK Report 2015-1, 2015.
- [15] Y. G. Cui, et al., Conceptual Design Report for Experimental Search for Lepton Flavor Violating  $\mu^- - e^-$  Conversion at Sensitivity of  $10^{-16}$  with a Slow-Extracted Bunched Proton Beam, KEK Report 2009-10, 2009.
- [16] L. Bartoszek, et al., Mu2e Technical Design Report, [arXiv:1501.05241](https://arxiv.org/abs/1501.05241), 2015.
- [17] J. E. Amaro, A. M. Lallena, J. Nieves, Radiative pion capture in nuclei: a continuum shell-model approach, *Nucl. Phys. A* 623 (3) (1997) 529 – 547.
- [18] A. Czarnecki, X. Garcia i Tormo, W. J. Marciano, Muon decay in orbit: Spectrum of high-energy electrons, *Phys. Rev. D* 84 (2011) 013006.
- [19] C. Höppner, et al., A novel generic framework for track fitting in complex detector systems, *Nucl. Instrum. Methods Phys. Res. A* 620 (23) (2010) 518 – 525.
- [20] H. Primakoff, Theory of Muon Capture, *Rev. Mod. Phys.* 31 (1959) 802–822.
- [21] M. Döbeli, et al., Radiative muon capture in nuclei, *Phys. Rev. C* 37 (1988) 1633 – 1646.
- [22] D. S. Armstrong, et al., Radiative muon capture on Al, Si, Ca, Mo, Sn, and Pb, *Phys. Rev. C* 46 (1992) 1094–1107.
- [23] P. C. Bergbusch, et al., Radiative muon capture on O, Al, Si, Ti, Zr, and Ag, *Phys. Rev. C* 59 (1999) 2853–2864.
- [24] P. Christillin, Radiative muon capture for  $N = Z$  nuclei, *Nucl. Phys. A* 362 (2) (1981) 391 – 404.
- [25] M. Gmitro, A. A. Ovchinnikova, T. V. Tetereva, Continuity-equation constraint in the two-vertex nuclear processes: Radiative muon capture on  $^{16}\text{O}$  and  $^{40}\text{Ca}$ , *Nucl. Phys. A* 453 (4) (1986) 685–706.
- [26] S. Agostinelli, et al., Geant4-a simulation toolkit, *Nucl. Instrum. Methods Phys. Res. A* 506 (3) (2003) 250 – 303.
- [27] M. Wang, et al., The Ame2012 atomic mass evaluation, *Chinese Physics C* 36 (12) (2012) 1603.
- [28] B. Macdonald, et al., Neutrons from Negative-Muon Capture, *Phys. Rev.* 139 (1965) B1253–B1263.
- [29] S. E. Sobottka, E. L. Wills, Energy Spectrum of Charged Particles Emitted Following Muon Capture in  $\text{Si}^{28}$ , *Phys. Rev. Lett.* 20 (1968) 596–598.
- [30] V. I. Komarov, O. V. Savchenko, *Sov. J. Nucl. Phys.* 8 (1969) 239.

- [31] D. F. Measday, The nuclear physics of muon capture, *Physics Reports* 354 (45) (2001) 243 – 409.
- [32] T. Suzuki, D. F. Measday, J. P. Roalsvig, Total nuclear capture rates for negative muons, *Phys. Rev. C* 35 (1987) 2212 – 2224.